PCCP

Accepted Manuscript

ROYAL SOCIETY OF CHEMISTRY

www.rsc.org/pccp

PCCP

ARTICLE

Assembly and Relaxation Behaviours of Phosphatidylethanolamine Monolayers investigated by Polarization and Frequency Resolved SFG-VS

Received 00th January 20xx,
Accepted 00th January 20xx

DOI: 10.1039/x0xx00000x

www.rsc.org/

Feng Wei, [a, †] Wei Xiong, [a] Wenhui Li, [a] Wangting Lu, [a] Heather C. Allen, [b] Wanquan Zheng [a, c]

Abstract The assembly conformation and kinetics of phosphatidylethanolamine(PE) lipids are the key to the membrane curvatures and activities such as exocytosis, endocytosis and Golgi membranes fusion. In the current study, a polarization and frequency resolved (bandwidth≈ 1 cm^{-1}) picosecond sum frequency generation (SFG) system was developed to characterize Phosphatidylethanolamine monolayers. In addition to obtaining π-A isotherms and Brewster angle microscopy (BAM) images, the conformational changes and assembly behaviors of phosphatidylethanolamine molecules are investigated by analyzing the SFG spectra collected at various surface pressure (SP). The compression kinetics and relaxation kinetics of Phosphatidylethanolamine monolayers are also reported. The conformational changes of PE molecules during the monolayer compression are separated into several stages: reorientation of head group PO_2^- in the beginning of liquid-expanded (LE) phase, conformational changes of head group alkyl chains in the LE phase, conformational changes of tail group alkyl chains in the LE-liquid condensed (LE-LC) phase. Such understanding may help researchers to effectively control the lipid molecular conformation and membrane curvatures during the exocytosis/endocytosis processes.

1 Introduction

Phosphatidylethanolamine (PE) is a critically important zwitterionic phospholipid within the cell membrane, and is the second most abundant phospholipid in mammalian cells, with an abundance of approximately 25%. The proportion of PE in brain can as much as 45%.[1] The inner membranes of mitochondria are also enriched in PE lipids compared to other membranes.[1] The decrease in PE proportion in the mitochondria membranes of yeast, T. brucei and in mammalian cells can greatly change the membrane morphologies.[2, 3] PE molecules are also frequently involved in many membrane activities such as, exocytosis, endocytosis and Golgi membrane fusion.[4-6] It has been reported that PE facilitates the exocytosis process and accelerates expulsion of a neurotransmitter in PC12 cells.[4] It also has been proposed that the lack of PE lipid may impair membrane fusion and cause inhibition of the cell cycle in parasite T. brucei.[3] Prevalent usages of PE in drug delivery and gene therapy as components of lipid raft or aerosol have been reported in the literatures.[7, 8] With the mediation of peptides, cholesterols, pH values and divalent ions, PE can facilitate the delivery of DNA and RNA molecules to target cell by membrane fusion and cell penetration.[9, 10] Yet, PE's specific role, or the exact mechanism of action, in these membrane activities is not fully understood yet.[11-15]

The assembly and relaxation behaviors of PE lipids are the key to their membrane activities.[12-14] The phase transition and assembly behaviors of lipid molecules in model systems of lipid monolayers, has been studied by characterizing techniques such as, Infrared reflection absorption spectroscopy (IRRAS),[16] Brewster angle microscopy (BAM),[9,16] and grazing incidence X-ray diffraction (GIXD).[12, 14] Sum frequency generation vibrational spectroscopy(SFG-VS) is a nonlinear vibrational spectroscopy with the merits of interface specificity and monolayer sensitivity,[17-19] which enable the characterization of structural and conformational changes of lipid molecules in the interfacial environment. Cholesterol induced condensation of DPPC (dipalmitoylphosphatidylcholine) monolayers has been elucidated by Bonn *et al.* via femto-second broad-band SFG-VS (BB-SFG-VS) based on the alkyl chain spectra (2700-3100 cm^{-1}).[20, 21] The conformation, surface orientation and hydration of deuterated DPPC tail and head groups has been characterized by Ma *et al.* via BB-SFG-VS.[22-24] SFG-VS is also capable of capturing the changes of ordering, hydration and orientations of lipid molecules during their interacting with ions, such as, Na^+, Ca^{2+} and Thiocyanate (SCN^-).[25-27] The Duramycin-lipid[28]

[a] Institution for Interdisciplinary research, Jianghan University, Zhuankou district, Wuhan, Hubei, China, 430056
[b] Department of Chemistry and Biochemistry, The Ohio State University, 100 West 18th Avenue, Columbus, OH 43210, USA
[c] Institut des Sciences Moléculaires d'Orsay, Université de Paris-Sud, 91405, ORSAY Cedex, France
† Corresponding Author: Email: weifeng@jhun.edu.cn, Address: Building J13, Room C202, 8th Triangle Lake Road, Zhuankou district, Wuhan, Hubei, China, 430056.
Electronic Supplementary Information (ESI) available: Details about π-A isotherm and BAM experiments, SFG data analysis.
See DOI: 10.1039/x0xx00000x

and DNA-lipid interactions[29] were also investigated via SFG-VS at the lipid monolayer/water interface. The influences of poly(ethylene oxide) chains to phase transitions behaviors of L-R-distearoyl phosphatidylethanolamine (DSPE) was investigated by C. Ohe etc. by BB-SFG-VS.[30] The interfacial conformations of phosphatidylethanolamine lipids are also investigated extensively by P. J. Kett *etc.*.[31-34] To understand the water molecular structures and orientations at lipid monolayer/water interface, new techniques such as, phase-sensitive BB-SFG-VS[35-37] and heterodyne-detected SFG-VS, [38] were also developed. In addition, polarization-resolved SFG-VS was also developed by Smits *et al.* to detect DPPC monolayer relaxation behaviors.[39, 40]

Most of above investigations are accomplished by BB-SFG-VS, with the spectra resolution more than 10 cm^{-1}, which is less than optimal to capture the structural details of lipids in the interface region. In the current study, a polarization and frequency resolved picosecond SFG system was developed to characterize the assembly and relaxation behaviors of PE lipid monolayers. The robustness of frequency-resolved SFG-VS in characterizing the structure and conformation details has already been shown by the investigations of 4-n-octyl-4-cyanobiphenyl (8CB), limonene and DMSO molecules at the interface.[41-44] The spectral resolution of the current SFG system is ≈ 1 cm^{-1}. With such a system, the assembly conformations and relaxation kinetics of PE molecules are characterized accurately and efficiently.

2 Experimental

The pico-second SFG system was purchased from EKSPLA, Lithuanian. Two laser beams at 1064nm with the pulse duration of 30 ps are generated from PL2251 mode-locked Nd:YAG laser. One of the 1064 nm beam (Amplified in PL2251, ≈33mJ, 20 Hz) is used to generate a first 532 nm beam for SFG-VS experiments, and a second 532 nm beam for optical parametric amplification (OPA), and 1064nm beam for differential frequency generation (DFG). The other 1064 nm beam (Train, 87.2MHz) is utilized to generate 532 nm train beam for synchronously pumped optical

parametric oscillator (OPO) system after amplification. The seed beam within the wavelength range of 680 nm-1064 nm with a bandwidth of < 0.2 nm (< 1.6 cm^{-1}) can be generated by the OPO system.[45] After the seed laser beam overlapping with the second 532 nm beam in OPA system and the 1064nm beam DFG system, the IR beam within the wavenumber range of 650-4000 cm^{-1} can be generated. The bandwidth of final IR beam is calculated to be ≈ 1 cm^{-1}, about twice of the transform-limited width of a 30 ps Guassian pulse (0.48 cm^{-1}). With such bandwidth, the SFG spectra distortion can be less than 1% in most molecular groups (shown in Table 1). At this level of spectra distortion, the intrinsic molecular lineshapes obtained by the current SFG system will provide better understanding of structural and conformational changes during the interfacial assembly of PE lipids.

Table 1. SFG spectra distortions at different bandwidths

$\Delta\nu_{H*}$	$\Delta\nu_{I}$	$\Delta\nu_{Instr}$	$\Delta\nu_{Voigt}$	Distortion
			Origin	Total	
4.7	8.1	5[a]	10.9	12.3	12.6%
		2[b]		11.1	2.2%
		1		11.0	0.5%
		0.55[c]		10.9	0.2%
3.1	6.5	5	8.3	10.0	20.1%
		2		8.6	3.5%
		1		8.4	0.9%
		0.55		8.3	0.3%

* All units in cm^{-1}. [a] and [b]: $\Delta\nu_{Instr}$ in most EKSPLA picosecond SFG systems, 2 cm^{-1} resolution can achieved in the wavenumber range of 3000-4000 cm^{-1}. [c]: $\Delta\nu_{Instr}$ reported in Ref. 42.

Scheme 1. Experimental setup of polarization-resolved SFG-VS detection. PS: polarization splitter, GP: Glan-laser polarizer, HWP: half-wave plate, F: filter, L: lens.

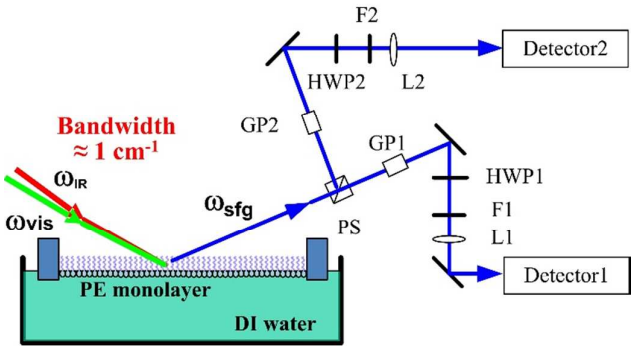

Polarization-resolved BB-SFG-VS detection has been shown previously by putting the polarization of the visible beam at 45° (or -45°) enabling separation of the signals at different polarizations with a polarization displacing prism.[39] Our approach in the pico-second SFG system slightly differs (check Scheme 1 for details). The ssp (The first "s" indicates that the detection polarization for SFG signal is S, The second "s" indicates that the incident visible beam is S-polarized, "p" indicates that the incident IR beam is P-polarized.) signal and ppp signal are separated by a polarization splitter, and the separated signals are detected by two sets of identical detection systems (Monochromator 3501/3504, SOLAR TII and PMT R7899, Hamatatsu) after the beams has gone through Glan polarizers, half-wave plates, filters and focusing lens separately. The polarization of the visible beam was changed by a motorized rotation stage.

The ssp and ppp spectra of PE monolayers were collected within the wavenumber range of 2800-3000 cm^{-1} and 1000-1200 cm^{-1} with a spectral resolution of 2 cm^{-1}. The visible beam and IR beam are focused to the air/water interface at incident angle of 63° and 52° respectively. The SFG signals of each wavenumber were averaged at least 150 times. The intensities of ssp and ppp spectra are calibrated by normalizing to z-cut quartz at rotational angle of 0° (which only have SFG response in the ssp and ppp polarization combinations). All the experiments are carried out in a controlled room environment (room temperature 22 ± 1 °C and humility less than 40%).

Phys. Chem. Chem. Phys. ARTICLE

Additional details of π-A isotherm and BAM experiments are described in Supporting Information.

3 Results and discussion

3.1 Isotherm and BAM images

Scheme 2. Molecular structures of PE molecules

DMPE (C_{14})

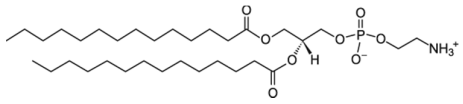

DPPE (C_{16})

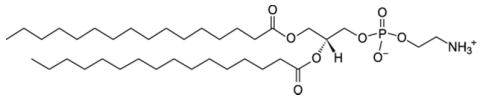

The π-A isotherm curves and BAM images of DMPE and DPPE monolayers are shown in Figure 1 (See SI for the experimental details of π-A isotherm and BAM images). As seen in Figure 1, the SP of DMPE monolayer rises at mean molecular area (MMA) of 76 Å^2, and reaches a plateau (SP = 6.5 ~ 10 mN/m) at molecular area of 56 Å^2 after going through the liquid-expanded (LE) phase. This plateau is also called LE-LC phase transition region. It should be noted that the rising point of SP in our experiments is smaller than that which is reported in previous literature (~ 82 Å^2); however, our experiments were conducted at 22 °C (smaller than the temperature of 25 °C reported in the literature).[46] After the gradual increase during the compression prior to and within the plateau area, the SP of the DMPE monolayer increases significantly at MMA of 35 Å^2 in the liquid-condensed (LC) phase. The SP of the DMPE monolayer then reaches a second plateau, which is called collapse phase, at a MMA of 28 Å^2. On the other hand, DPPE monolayer show much less compression elasticity. The SP of the DPPE monolayer rises at MMA of 58 Å^2, and continues straightly through LE and LC phase to the collapse phase at a MMA of 42 Å^2.

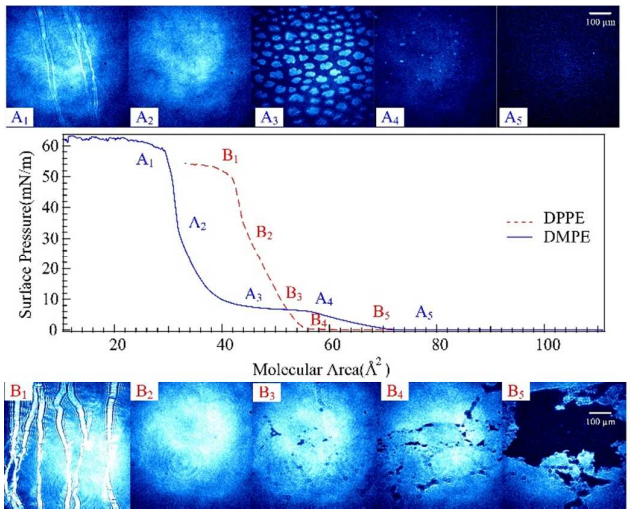

Figure 1. π-A isotherm curves and BAM images of DMPE (blue solid line) and DPPE (red dashed line) monolayer at collapse phase (A_1, B_1), LC phase(A_2, B_2), LE-LC phase(A_3, B_3), LE phase(A_4, B_4) and Gas-LE phase(A_5, B_5).

Table 2. The molecular area and surface pressures where the BAM images were taken.

	DMPE monolayer			DPPE monolayer	
	MMA(Å^2)	SP(mN/m)		MMA(Å^2)	SP(mN/m)
A_5	80	0.033	B_5	82.0	0.022
A_4	58.6	5.0	B_4	61.0	0.19
A_3	52.7	6.6	B_3	52.0	7.1
A_2	33.2	26.2	B_2	45.0	30.4
A_1	20.7	62.5	B_1	36.1	53.8

The BAM images of DMPE and DPPE monolayer at the point of collapse (A_1, B_1), in LC (A_2, B_2), LE-LC (A_3, B_3), LE (A_4, B_4) and Gas-LE (A_5, B_5) phases are also shown in Figure 1. As seen in Figure 1, the BAM images of DMPE and DPPE monolayers at collapse phase and LC phase are almost identical, and those in the LE-LC, LE and Gas-LE phases are different. Liquid-like domains with round edges are shown in BAM image (A_5) of Gas-LE phase of DMPE monolayer. As for the DPPE monolayer, the solid-like domains with sharp edges are mostly observed in the Gas-LE phase. It is clear that the brightness of domains in the DPPE BAM image are much higher than that of DMPE BAM image, revealing the smaller thickness of the DMPE domains. The DMPE monolayer show multiple lobular-like domains in the LE-LC phase, which is consistent with BAM results in previous reports. The brightness of such lobular-like domains of DMPE are similar with that of the DPPE monolayer in Gas-LE phase, indicating their thicknesses are similar.[47] By comparing the brightness of different BAM images in different phases, it can be concluded that the thickness of the DMPE monolayer increases in LE-LC phase by forming multiple domain during the compression, but the thickness of the DPPE monolayer does not change too much (which consistent with its lower compression elasticity).

3.2 Conformational changes of PE alkyl chains

Both ssp spectra and ppp spectra of the lipid monolayers were collected simultaneously by setting the polarization angle of the visible beam to 45°. The influences of environmental changes, such as sample dehydration and water height level, to the intensities of ssp and ppp spectra can be ruled out by such geometry. However, it should be noted that the SFG intensities collected from two detectors under such geometry are actually $I_1(\Omega = 45^\circ) = C_1\left|\chi^{(2)}_{ssp} + \chi^{(2)}_{spp}\right|^2$ and $I_2(\Omega = 45^\circ) = C_2\left|\chi^{(2)}_{psp} + \chi^{(2)}_{ppp}\right|^2$.[48] Due to the isotropic structure of the lipid monolayer at air/water interface, the contribution of $\chi^{(2)}_{spp}$ and $\chi^{(2)}_{psp}$ in these two formulas can be neglected and gives: $I_1 \approx C_1\left|\chi^{(2)}_{ssp}\right|^2$ and $I_2 \approx C_2\left|\chi^{(2)}_{ppp}\right|^2$. The SFG intensities of the DMPE monolayer at Ω=45 ° and Ω=-45° were also collected by switching the polarization angle back and forth at each wavenumber. The calculated SFG intensity differences

$R = \frac{\Delta I}{I} = \frac{I(\Omega = 45^\circ) - I(\Omega = -45^\circ)}{I(\Omega = 45^\circ) + I(\Omega = -45^\circ)}$ are very small, which indicate negligible contribution from $\chi^{(2)}_{psp}$ and $\chi^{(2)}_{spp}$ in SFG spectra collected at Ω = ±45 ° and the validation of the simplified formulas above.

3.2.1 SFG spectra at different SP

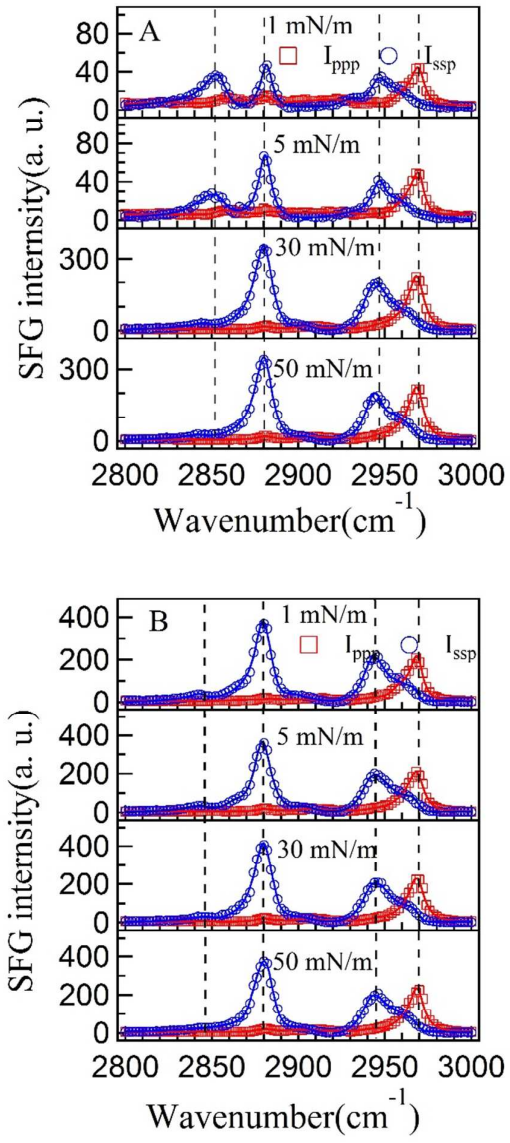

Figure 2. SFG spectra of A). DMPE monolayer and B). DPPE monolayer at SP = 1 mN/m, 5 mN/m, 30 mN/m and 50 mN/m in the wavenumber range of 2800-3000 cm^{-1}.

Figure 2 shows the SFG spectra of the DMPE and DPPE monolayer at surface pressure of 1 mN/m, 5 mN/m, 30 mN/m and 50 mN/m in the wavenumber range of 2800-3000 cm^{-1}. The vibrational peaks within this range mostly originate from CH_2 and CH_3 groups in alkyl chains of the phospholipids. As seen in Figure 2, DMPE and DPPE monolayer show multiple characteristic peaks: CH_2-SS-trans (~ 2840 cm^{-1}, ~ 2905 cm^{-1}), CH_2-SS-gauche (~ 2850 cm^{-1}, ~ 2925 cm^{-1}), CH_3-SS (~ 2880 cm^{-1}), CH_3-Fermi (~ 2945 cm^{-1}), CH_3-AS (~ 2970 cm^{-1}).[22, 23] It should also be noted that the small peak observed at ~ 2905 cm^{-1} (~ 2925 cm^{-1} at lower SP) can be assigned to either CH group, CH_2 groups in head groups (glycerol backbone, choline group). Such small peak is also observed in the SFG spectra of an ODT monolayer (with no C-H group) at surface pressure of 5 mN/m and 30 mN/m (shown in Figure S1). Thus the peak at ~ 2905 cm^{-1} should be assigned to CH_2 groups.

By comparing the SFG spectra of the DMPE and DPPE monolayers at different SP, it is easy to notice that all the spectra of the DPPE monolayers are very similar while the spectra of the DMPE monolayer at SP = 1 mN/m and 5 mN/m are different from the spectra at other SP. All the SFG spectra of the DPPE monolayers show very small contribution of the CH_2-SS-trans peak at 2840 cm^{-1}, which indicates the alkyl chains of DPPE molecules are well ordered from a very low SP. The similarity between SFG spectra also indicate the conformation DPPE molecules are alike in different SP, which consistent with their lower compression elasticity comparing to DMPE molecules. As with DMPE monolayers, the differences between the SFG spectra at various SP indicates DMPE molecules undergo much more conformational changes during the compression. The spectra collected at SP = 1 mN/m and 5 mN/m (below the first plateau) show significant contribution from the CH_2-SS peaks. The fitted widths of the CH_2-SS-trans in the tail groups and head groups are 36.0 ± 9.3cm^{-1} and 20.0 ± 6.8 cm^{-1} respectively at SP=1 mN/m. The peaks of CH_2-SS-gauche in tail groups and head groups are clearly seen in the spectra. Such spectroscopic characteristics indicate the alkyl chains in the tail groups and head groups of DMPE molecules are randomly ordered or in a coiled conformation. Such conformation also leads to much lower SFG intensities of the CH_3 group related peaks (CH_3-SS, CH_3-fermi, CH_3-AS) compared to the intensities of the DPPE monolayer. Such conformation should be the main reason that the DMPE BAM images show lower brightness in the LE phase. As the SP increase to 5 mN/m, the peak of CH_2-SS-gauche in tail groups remains visible but the peak in head groups are not seen from the spectra. The peak widths of CH_2-SS-trans in tail groups and head groups are 16.6 ± 4.1 cm^{-1} and 9.5 ± 2.6 cm^{-1} respectively.

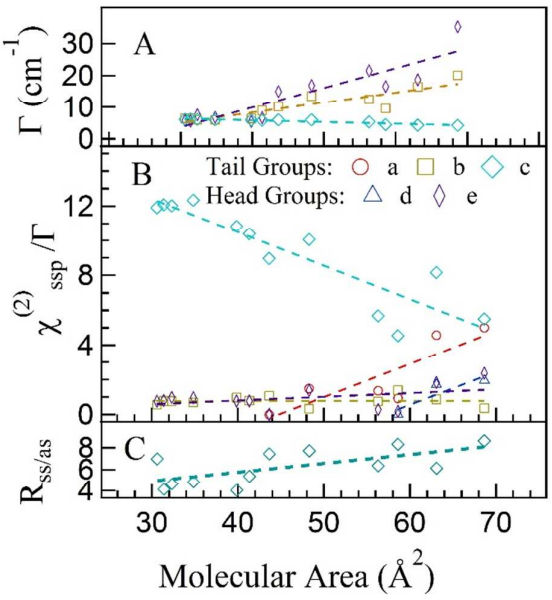

Figure 3. The fitting results of SFG spectra of the DMPE monolayers at various SP. A). Peak widths (Γ) of different vibration modes. B). Peak amplitude ($\chi^{(2)}_{ssp}/\Gamma$) of different vibration modes calculated from the fitting results, C). Susceptibility ratio ($R_{ss/as} = \chi^{(2)}_{ssp,CH_3\text{-}ss} / \chi^{(2)}_{ssp,CH_3\text{-}as}$) of methyl groups calculated from the fitting results. Tail groups: a. CH_2-SS-gauche, b. CH_2-SS-trans, c. CH_3-SS, Head groups: d. CH_2-SS-gauche, e. CH_2-SS-trans.

The conformational changes of the DMPE molecules can also quantified by the fitting results of the SFG spectra of the DMPE monolayers at various SP shown in Figure 3. As seen in Figure 3, the widths of the CH_2-trans peaks in the tail and head groups decrease as the MMA decreases, while the width of CH_3-SS peak increases as the MMA decreases upon compression. Such changes indicate that the conformation of the CH_2 groups become more rigid while the conformation of the CH_3 groups become less rigid during the compression. The peak amplitude of CH_3-SS mode increases and the susceptibility ratio of $R_{ss/as} = \chi^{(2)}_{ssp,CH_3\text{-}ss} / \chi^{(2)}_{ssp,CH_3\text{-}as}$ decreases as the MMA decreases. The peak width difference of the CH_3-SS mode between the LE phase (4.9 ± 0.2 cm^{-1}) and the LC phase (6.2 ± 0.1 cm^{-1}) also indicate that the tail group alkyl chain may adopt coiled conformation rather than randomly ordered conformation. If we assume the all-trans conformations are rigidly formed in LC phase, the chain tilt angle α with respect to the surface normal can be calculated by $\alpha = 41.5° - \theta_{CH_3}$. The value of α is calculated to be 13.5 ± 1.8° at high SP.[22, 24, 49-51] The peak amplitudes of CH_2 groups (both CH_2-SS-trans and CH_2-SS-gauche) decrease as the MMA decreases. The disappearing of tail group CH_2-SS-gauche mode and head group CH_2-SS-gauche mode at different MMA indicate that the conformational changes of the DMPE alkyl chains have separated stages: the reorientation of head group alkyl chains mostly happen in the LE phase, the reorientation of tail group alkyl chains in mostly happen in the LE-LC phase.

3.2.2 Conformational changes of DMPE molecules in LE-LC phase

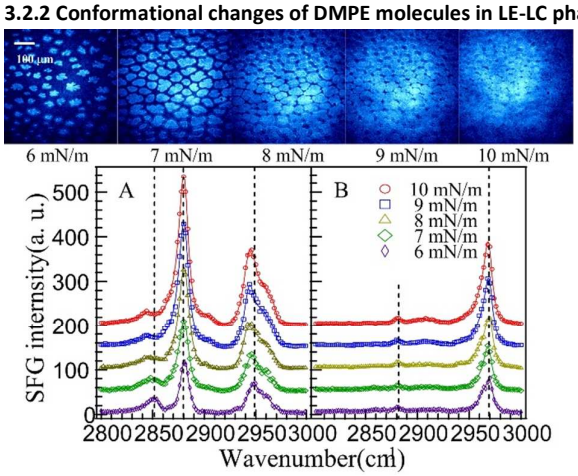

Figure 4. BAM images and SFG spectra of DMPE monolayers at SP = 6, 7, 8, 9, 10 mN/m. A). ssp spectra; B). ppp spectra.

The lipid conformations and molecular interactions in LE-LC phase are very important to membrane activities. The interaction between the LC and LE domains in the LE-LC phase were proven responsible for the double layer formation and squeezing out mechanism of Lung surfactant (DPPC).[52, 53] BAM images and SFG spectra of the DMPE monolayers at SP = 6, 7, 8, 9, 10 mN/m (LE-LC phase) are shown in Figure 4. Observed from Figure 4, the bright domains in the DMPE BAM images become bigger as the SP increases from 6 mN/m to 10 mN/m, indicating an increasing phase transition percentage of the DMPE monolayer during compression. The amplitude of the CH_3-SS, CH_3-Fermi, CH_3-AS peaks increases gradually and the amplitude of the CH_2-SS-trans peak at 2840 cm^{-1} become relatively smaller, which indicates the ordering of alkyl chains has increased. The fitting result shows the amplitude of the CH_2-SS-gauche peak in tail groups reduces to zero at SP = 9 mN/m, indicating that the tail group alkyl chains of DMPE molecules are fully stretched (all-trans). The fully extended alkyl chains also result in smaller inter-molecular distance and larger adhesive *van der waals* force between DMPE molecules, as well as the formation of multiple lobed-shaped domains in BAM images of DMPE monolayer. Additionally, $\omega_{0,CH_3-Fermi}$ is downshifted about 4.6 ± 0.5 cm^{-1} as the SP of DMPE monolayer increases from 6 to 10 mN/m. As discussed in the literatures, the CH_3-Fermi mode is generated by the energy level splitting of CH_3-SS mode and the second overtone of CH_3-bending mode, whose energy levels are very close to each other.[54, 55] The decrease in the peak center wavenumber of CH_3-Fermi mode indicate the energy level of CH_3-bending mode (second overtone) is lowered. The adhesive *van der waals* force between the fully extended alkyl chains should be the main reason to the weakening of vibrational force constant (*k*) of CH_3-bending mode and the redshift of $\omega_{0,CH_3\text{-}Fermi}$. A similar redshift of $\omega_{0,Free-OH}$ ($\Delta\omega_0 = -20cm^{-1}$) was also observed at water/OTS monolayer interface comparing to the water/air interface.[56-58]

Additionally, the peak amplitude ratio between the CH_3-SS and CH_3-Fermi peaks ($R_{Fermi} = \frac{\chi^{(2)}_{CH_3\text{-}SS} / \Gamma_{CH_3\text{-}SS}}{\chi^{(2)}_{CH_3\text{-}Fermi} / \Gamma_{CH_3\text{-}Fermi}}$) increases as the SP increases, but $\omega_{0,CH_3\text{-}SS}$ does not change significantly ($\Delta\omega_{0,CH_3\text{-}SS}$ = −0.4 ± 0.2 cm^{-1}) comparing to the downshifting of $\omega_{0,CH_3\text{-}Fermi}$. These

experimental results indicate either the contribution from Fermi resonance generated CH_3-SS peak is very small, or the influence of Fermi resonance effects to $\omega_{0,CH_3\text{-SS}}$ is compensate by the effects of the adhesive *van der waals* forces. Further experiments are required to give a quantitative evaluation of the influences of the Fermi resonance effect to the frequency and amplitude of CH_3-SS mode, as well as the *van der waals* interactions between CH_3 groups.

3.3 Conformational changes of PO_2^- group

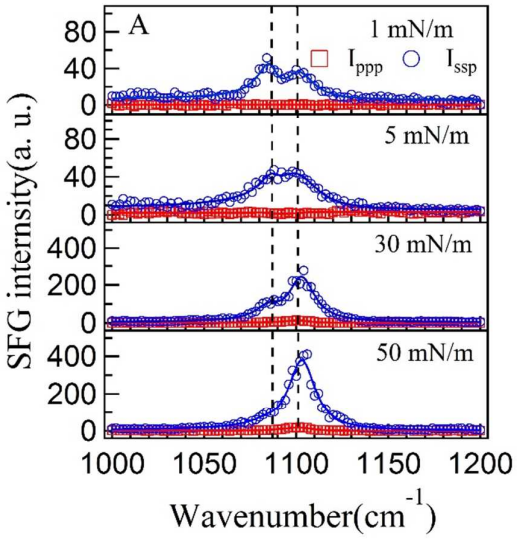

Figure 5. SFG spectra of A). DMPE monolayer and B). DPPE monolayer at SP = 1 mN/m, 5 mN/m, 30 mN/m and 50 mN/m in the wavenumber range of 1000-1200 cm^{-1}.

Figure 5 shows SFG spectra of DMPE and DPPE monolayers at SP = 1 mN/m, 5 mN/m, 30 mN/m and 50 mN/m in the wavenumber range of 1000-1200 cm^{-1}. Two characteristic peaks are observed at ~ 1085 cm^{-1} and ~ 1100 cm^{-1}, which originate from the R-O-P-O-R groups and PO_2^- groups (symmetric stretching) respectively. Although the peak of C-OP at ~ 1050 cm^{-1}, which has been reported by Ma, G. *etc.* in previous literature, is too weak to be observed. It also has been reported that the peak positions of the PO_2^--SS mode are very sensitive to the hydration state of lipid head groups. The fitting results of SFG spectra indicate small blue-shifts of PO_2^--SS peaks $\Delta\omega_{0,PO_2\text{-SS}}$ = 2.1 ± 0.5 cm^{-1} when the SP increases, which indicate that the hydration states of PO_2^- groups should be slightly changed. Similar phenomena were also observed by Ma, G. *etc.* using BB-SFG-VS in DPPC monolayers.[22, 24]

The fitting results of SFG spectra also indicate that susceptibility ratios $R_{PO_2^-} = \chi^{(2)}_{ppp,PO_2^-\text{-ss}} / \chi^{(2)}_{ssp,PO_2^-\text{-ss}}$ of DMPE and DPPE monolayers increases as the SP increases. The tilt angle dependence of $R_{PO_2^-}$ are plotted in Figure S3. According to our data, the tilt angles of PO_2^- groups in DMPE molecule and DPPE molecule at SP = 1 mN/m are close to 26°. And the tilt angles of PO_2^- groups of DMPE and DPPE monolayers at SP = 50 mN/m are 54.1 ± 6.8° and 46.8 ± 5.4° respectively.

3.4 Compression kinetics of PE monolayer

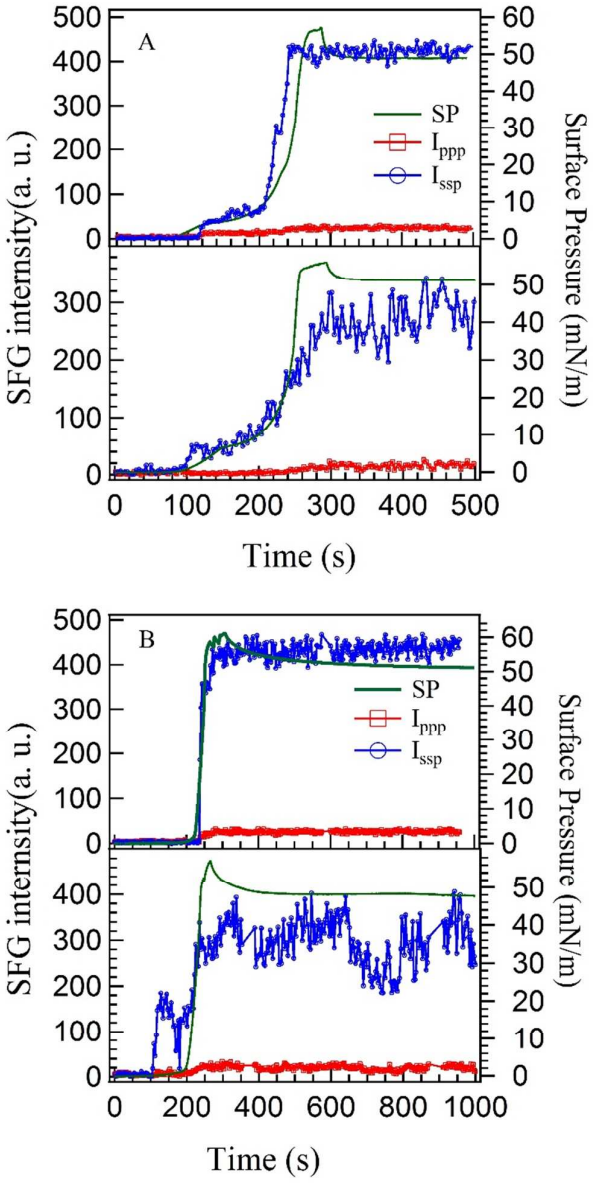

Figure 6. Compression kinetics of A). DMPE monolayer and B). DPPE monolayer monitored by SP sensor and polarization-resolved SFG system. Compression speed: 27 mm/min. Compressions stopped at ~ 60 mN/m. The SFG signals of both ssp and ppp polarizations were collected at 2970 cm^{-1} (upper) and 1105 cm^{-1} (bottom) by averaging 50 pulses.

The current polarization resolved SFG system is also capable of obtaining both molecular abundance and orientation based on the simultaneously collected ssp and ppp signals.[59-61] Such information can give a rough and quick estimation of molecular changes in the time domain, which would be very useful for understanding the kinetics of reaction, adsorption and desorption processes at the interface. Figure 6 shows the compression kinetics of DMPE and DPPE monolayer monitored by the SP sensor and the polarization-resolved SFG system. The monitoring wavenumbers were 2970 cm^{-1} and 1105 cm^{-1}, which correspond to characteristic vibrational peaks of the CH_3-AS and PO_2^--SS modes respectively. As seen in Figure 6, the increasing of SP of DMPE and DPPE monolayers under a compression speed of 27 mm/min follow the similar trend as the SP increasing in the π-A isotherms (which were collected under compression speed of 5 mm/min). The plateau area of the DMPE monolayer at ~ 6 mN/m is also shown in Figure 4A. The changing of $I^{2970cm^{-1}}$ from the DMPE monolayer can be separated into several stages: The first significant increase occurs at the end of LE phase, followed by a gradual rise in LE-LC phase, the second significant increase in the LC phase and the final plateau area at the end of LC phase. It is interesting to note that the final plateau area of $I^{2970cm^{-1}}$ occurs at SP = 27 mN/m, which is much earlier than the final plateau of SP at ~ 55 mN/m. The fitted amplitudes of CH_3-SS mode at various SP in Figure 3 show a similar trend. Such phenomena indicate that the conformation of the DMPE tail groups reaches equilibrium after SP reaches 27 mN/m (at the beginning of LC phase). BAM images of DMPE monolayers in LC phase (shown in Figure 1) indicate that the DMPE molecules are packing closely to form a monolayer with unified thickness. It is interesting that the surface pressure of most cell membranes also maintain at ~ 30 mN/m. It has been reported that the phospholipids monolayer at such SP can create an integral and elastic hydrophobic environment for protein insertion and functioning.[62] Cell membrane at such equilibrium state also provide a desirable barrier to separate the cellular activities from the influences of the extra-cellular environments. On the other hand, the changing of $I^{1105cm^{-1}}$ from the DMPE monolayer is a little different: the first significant increase occurs at the beginning of LE phase, and the final plateau area of $I^{1105cm^{-1}}$ occurs later than the final plateau area of the SP. It is understandable because the head groups of lipid molecules are usually placed at exterior areas of cell membranes, which are more susceptible to the environments. Similar trends are also seen in Figure 6B, which presents the compression kinetics of the DPPE monolayer at 2970 cm^{-1} and 1105 cm^{-1}.

The calculated SFG intensity ratios $R^{1105cm^{-1}} = I_{ssp}^{1105cm^{-1}} / I_{ppp}^{1105cm^{-1}}$ and $R^{2970cm^{-1}} = I_{ssp}^{2970cm^{-1}} / I_{ppp}^{2970cm^{-1}}$ are shown in Figure S4. Despite the small contributions from non-resonant susceptibilities and other peaks ($I^{2970cm^{-1}} = C|\chi_{NR} + \chi_{CH_3\text{-Fermi}}^{2970cm^{-1}} + \chi_{CH_3\text{-AS}}^{2970cm^{-1}}|^2$ and $I^{1105cm^{-1}} = C|\chi_{NR} + \chi_{R\text{-O-P-O-R}}^{1105cm^{-1}} + \chi_{PO_2\text{-SS}}^{1105cm^{-1}}|^2$), the SFG intensities ratios gives a qualitative evaluation of tilt angle changes of CH_3 groups. The rising points of $R^{1105cm^{-1}}$ and $R^{2970cm^{-1}}$ are clearly separated from the rising point from the SP curve. The difference between the compression kinetics of the PE monolayers detected at 2970 cm^{-1} and 1105 cm^{-1} indicate that the reorientation of PO_2^- groups (head groups) and -CH_3 groups (tail groups) occur separately during the compression.

3.5 Relaxation kinetics of PE monolayers at high SP

Figure 6 also shows the relaxation kinetics of PE monolayers after the compression stopped at SP ≈ 60 mN/m. The decreasing curves of SP were fitted to single exponential decay curve: $SP(t) = SP_0 + A\exp\{\frac{t-t_0}{\tau}\}$. The fitting gives τ = 7-10 *s* for the DMPE monolayer and τ = 50-60 *s* for the DPPE monolayer. Such difference in relaxation kinetics may either be due to different mobility or different molecular interactions of DMPE and DPPE

molecules at high SP. On the other hand, it is interesting to see that the values of $I_{CH_3\text{-}AS}^{2970cm^{-1}}$ remain stable despite the significant decrease of SP after stopping the compression. Such information implies that the conformation of alkyl chains of PE molecules may remain stable during the monolayer relaxation, compatible with the experiment results mentioned above. This is possible because the molecular waist of the phospholipids is at the glycol groups, and not at the tail group alkyl chains. The molecular conformation of the phospholipids during the relaxation require additional elucidations which will be addressed in our further publications.

Conclusions

In this study, the conformational changes and assembly behaviors of DMPE and DPPE molecules are investigated by a frequency-resolved and polarization-resolved picosecond SFG-VS system, combined with the π-A isotherm and BAM detections. The compression kinetics and relaxation kinetics of PE monolayers are also measured. It is shown that the peak shift within few wavenumbers can be recognized by the current frequency-resolved SFG system. Base on the fitting parameters, the detailed conformational changes in methyl groups and dehydration of phosphate groups can be identified by such SFG system. Although, the signal noise ratio is not good enough to distinguish the contributions of homogeneous and inhomogeneous lineshape broadening from the fitting results.

Scheme 3 Schematic illustration of conformational changes of DMPE molecules at air/water interface.

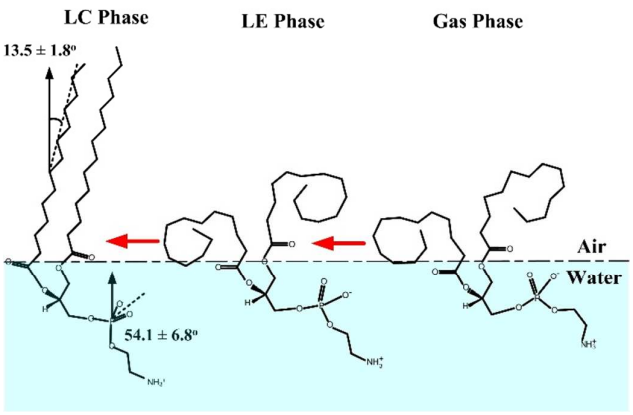

It is revealed that the conformational changes of DMPE molecules during the monolayer compression could be separated into several stages: reorientation of PO_2^- group in head group at the beginning of LE phase, conformational changes of head group alkyl chains (choline group) in the LE phase, conformational changes of tail group alkyl chains in the LE-LC phase. The conformational changes of DMPE molecules at the air/water interface are illustrated in Scheme 3. It has been reported that PE lipids tend to form non-lamellar membrane structures during the membrane fusion. After the reorientation of head group alkyl chains in the LE phase, the cone-shaped DMPE molecules may modulates membrane curvature and facilitate the formation of non-lamellar phases of the cell membranes during the exocytosis/endocytosis processes. Current research is the first step to understand the exocytosis behaviors and assembly behaviors of phosphatidylethanolamine (PE) molecules. The fine spectral resolution of our SFG system allow us to distinguish the head groups and tail groups of PE molecules, thus enable us to understand its molecular behaviors during the formation of the exocytosis vesicles or the PE-DNA complexes. The understandings about compression kinetics and relaxation kinetics of PE lipids will also help researchers to effectively control the lipid molecular conformation and membrane curvatures.

Acknowledgements

This work was supported by the Doctoral Program Foundation of Jianghan University (No. 1019-06100001).

Notes and references

1 J. E. Vance and G. Tasseva, *Biochim. Biophys. Acta,* 2013, **1831**, 543-554.
2 R. Steenbergen, *J. Bio. Chem.,* 2005, **280**, 40032-40040.
3 A. Signorell, E. Gluenz, J. Rettig, A. Schneider, M. K. Shaw, K. Gull and P. Bütikofer, *Mol. Micro.,* 2009, **72**, 1068-1079.
4 Y. Uchiyama, M. M. Maxson, T. Sawada, A. Nakano and A. G. Ewing, *Brain Res.,* 2007, **1151**, 46-54.
5 H. Chakraborty, T. Sengupta and Barry R. Lentz, *Biophys. J.,* 2014, ***107***, 1327-1338.
6 E. I. Pécheur, I. Martin, O. Maier, U. Bakowsky, J. M. Ruysschaert and D. Hoekstra, *Biochemistry,* 2002, ***41***, 9813-9823.
7 M. Schalke and M. Lösche, *Adv. Col. Interface Sci.,* 2000, ***88***, 243-274.
8 L. C. Gomes-da-Silva, N. A. Fonseca, V. Moura, M. C. Pedroso de Lima, S. Simoes and J. N. Moreira, *Acc. Chem. Res.,* 2012, ***45***, 1163-1171.
9 S. Gromelski and G. Brezesinski, *Phys. Chem. Chem. Phys.,* 2004, ***6***, 5551-5556.
10 M. A. Churchward, T. Rogasevskaia, D. M. Brandman, H. Khosravani, P. Nava, J. K. Atkinson and J. R. Coorssen, *Biophys. J.,* 2008, ***94***, 3976-3986.
11 M. Langecker, V. Arnaut, J. List and F. C. Simmel, *Acc. Chem. Res.,* 2014, ***47***, 1807-1815.
12 A. Zitzer, R. Bittman, C. A. Verbicky, R. K. Erukulla, S. Bhakdi, S. Weis, A. Valeva and M. Palmer, *J. Biol. Chem.,* 2001, ***276***, 14628-14633.
13 C. A. Helm, P. Tippmann-Krayer, H. Möhwald, J. Als-Nielsen and K. Kjaer, *Biophys. J.,* 1991, ***60***, 1457-1476.
14 X. Wang, H. Takahashi, I. Hatta and P. J. Quinn, *Biochim. Biophys. Acta,* 1999, **1418**, 335-343.
15 K. Czapla, B. Korchowiec and E. Rogalska, *Langmuir,* 2010, **26**, 3485-3492.
16 S. Gromelski and G. Brezesinski, *Langmuir,* 2006, **22**, 6293-6301.
17 X. D. Zhu, H. Suhr and Y. R. Shen, *Phys. Rev. B,* 1987, **35**, 3047–3050.
18 A. L. Harris, C. E. D. Chidsey, N. J. Levinos and D. N. Loiacono, *Chem. Phys. Lett.,* 1987, **141**, 350–356.
19 Y. R. Shen, *Nature*, 1989, **337**, 519–525.
20 S. Roke, J. Schins, M. Muller and M. Bonn, *Phys. Rev. Lett.,* 2003, **90**, 128101.
21 M. Bonn, S. Roke, O. Berg, Juurlink, A. Stamouli and M. Müller, *J. Phys. Chem. B,* 2004, **108**, 19083-19085.

22 G. Ma and H. C. Allen, *Langmuir,* 2006, **22**, 5341-5349.
23 G. Ma and H. C. Allen, *Langmuir,* 2006, **22**, 11267-11274.
24 G. Ma and H. C. Allen, *Langmuir,* 2007, **23**, 589-597.
25 N. N. Casillas-Ituarte, X. Chen, H. Castada and H. C. Allen, *J. Phys. Chem. B,* 2010, **114**, 9485-9495.
26 M. Sovago, G. W. Wurpel, M. Smits, M. Muller and M. Bonn, *J. Am. Chem. Soc.,* 2007, **129**, 11079-11084.
27 P. Viswanath, A. Aroti, H. Motschmann and E. Leontidis, *J. Phys. Chem. B,* 2009, **113**, 14816-14823.
28 G. W. Wurpel, M. Sovago and M. Bonn, *J. Am. Chem. Soc.,* 2007, **129**, 8420-8421.
29 I. I. Rzeznicka, M. Sovago, E. H. G. Backus, M. Bonn, T. Yamada, T. Kobayashi and M. Kawai, *Langmuir,* 2010, **26**, 16055-16062.
30 C. Ohe, Y. Goto, M. Noi, M. Arai, H. Kamijo and K. Itoh, *J. Phys. Chem. B,* 2007, **111**, 1693-1700.
31 P. J. Kett, M. T. Casford and P. B. Davies, *Langmuir,* 2010, **26**, 9710-9719.
32 P. J. Kett, M. T. Casford and P. B. Davies, *J. Phys. Chem. B,* 2011, **115**, 6465-6473.
33 P. J. Kett, M. T. Casford and P. B. Davies, *J. Chem. Phys.,* 2013, **138**, 225101.
34 P. J. Kett, M. T. Casford and P. B. Davies, *J. Phys. Chem. B,* 2013, **117**, 6455-6465.
35 I. V. Stiopkin, H. D. Jayathilake, A. N. Bordenyuk and A. V. Benderskii, *J. Am. Chem. Soc.,* 2008, ***130***, 2271-2275.
36 M. Sovago, E. Vartiainen and M. Bonn, *J. Chem. Phys.,* 2009, **131**, 161107.
37 X. Chen, W. Hua, Z. Huang and H. C. Allen, *J. Am. Chem. Soc.,* 2010, **132**, 11336-11342.
38 J. A. Mondal, S. Nihonyanagi, S. Yamaguchi and T. Tahara, *J. Am. Chem. Soc.,* 2010, **132**, 10656-10657.
39 M. Smits, M. Sovago, G. W. H. Wurpel, D. Kim, M. Muller and M. Bonn, *J. Phys. Chem. C,* 2007, **111**, 8878-8883.
40 S. Yamamoto, A. Ghosh, H. K. Nienhuys and M. Bonn, *Phys. Chem. Chem. Phys.,* 2010, **12**, 12909-12918.
41 L. Fu, Y. Zhang, Z. H. Wei and H. F. Wang, *Chirality,* 2014, **26**, 509-520.
42 L. Velarde and H. F. Wang, *J. Chem. Phys.,* 2013, **139**, 084204.
43 L. Velarde and H. F. Wang, *Phys. Chem. Chem. Phys.,* 2013, **15**, 19970-19984.
44 L. Velarde and H. F. Wang, *Chem. Phys. Lett.,* 2013, **585**, 42-48.
45 B. C. Johnson, V. J. Newell, J. B. Clark and E. S. McPhee, *J. Opt. Soc. Am. B,* 1995, **12**, 2122-2127.
46 K. Hoda, Y. Ikeda, H. Kawasaki, K. Yamada, R. Higuchi and O. Shibata, *Colloids. Surf. B,* 2006, **52**, 57-75.
47 M. Minones, O. Conde, J. M. Trillo and J. Minones, *J. Phys. Chem. B,* 2010, **114**, 10774-10781.
48 F. Wei, Y. Y. Xu, Y. Guo, S. L. Liu and H. F. Wang, *Chin. J. Chem. Phys.,* 2009, **22**, 592-600.
49 W. Gan, B. H. Wu, Z. Zhang, Y. Guo and H. F. Wang, *J. Phys. Chem. C,* 2007, **111**, 8716-8725.
50 W. Gan, Z. Zhang, R. R. Feng and H. F. Wang, *J. Phys. Chem. C,* 2007, **111**, 8726-8738.
51 H. F. Wang, W. Gan, R. Lu, Y. Rao and B. H. Wu, *Int. Rev. Phys. Chem.,* 2005, **24**, 191-256.
52 I. C. Shieh and J. A. Zasadzinski, *P. Natl. Acad. Sci. USA,* 2015, **112**, E826-835.
53 P. Dhar, E. Eck, J. N. Israelachvili, D. W. Lee, Y. Min, A. Ramachandran, A. J. Waring and J. A. Zasadzinski, *Biophys. J.,* 2012, **102**, 56-65.
54 T. W. Zerda, M. Bradley and J. Jonas, *Chem. Phys. Lett.,* 1985, **117**, 566-570.
55 J. C. Lavalley and N. Sheppard, *Spectrochim. Acta A,* 1972, **28**, 2091-2101.
56 C. S. Tian and Y. R. Shen, *P. Natl. Acad. Sci. U. S. A. ,* 2009, **106**, 15148-15153.
57 L. F. Scatena, M. G. Brown and G. L. Richmond, *Science,* 2001, **292**, 908-912.
58 F. W. Delrio, M. P. de Boer, J. A. Knapp, E. David Reedy, Jr., P. J. Clews and M. L. Dunn, *Nat. Mater.,* 2005, **4**, 629-634.
59 X. Chen, J. Wang, C. B. Kristalyn and Z. Chen, *Biophys. J,* 2007, **93**, 866-875.
60 F. Wei and S. J. Ye, *J. Phys. Chem. C,* 2012, **116**, 16553-16560.
61 F. Wei, S. Ye, H. Li and Y. Luo, *J. Phys. Chem. C,* 2013, **117**, 11095-11103.
62 D. Marsh, *Biophys. J.,* 2007, ***93***, 3884-3899.